Radionuclide concentration and radon exhalation in new mix design of bricks produced reusing NORM by-products: The influence of mineralogy and texture

# Radionuclide concentration and radon exhalation in new mix design of bricks produced reusing NORM by-products: the influence of mineralogy and texture.

Chiara Coletti[1], Erika Brattich[2], Giorgia Cinelli[3], Giuseppe Cultrone[4], Lara Maritan[1], Claudio Mazzoli[1], Domiziano Mostacci[5], Laura Tositti[6], Raffaele Sassi[1]

[1] Department of Geosciences, University of Padova, Via Gradenigo 6, 25131 Padova, Italy

[2] Department of Physics and Astronomy, University of Bologna, via Irnerio 46, 40126 Bologna, Italy

[3] European Commission, Joint Research Centre (JRC), Via Enrico Fermi 2749, 21027 Ispra VA, Italy

[4] Department of Mineralogy and Petrology, Faculty of Science, University of Granada, Fuentenueva s/n, 18002 Granada, Spain

[5] Department of Industrial Engineering, University of Bologna, Via dei Colli 16, 40136 Bologna, Italy

[6] Department of Chemistry "G. Ciamician", University of Bologna, Via Selmi 2, 40126 Bologna, Italy

## Abstract

Many industrial by-products contain Naturally Occurring Radioactive Materials (NORM) that normally represent a cost in terms of monitoring, risk management and storage. When included in new mix designs of bricks, these materials may become a valuable sustainable resource. Before marketing, companies involved in development and commercialization of these new building materials ensure safety related to radiation, usually by assessing radon-related risk. According to the Council Directive 2013/59/Euratom, both raw materials and final products used in building constructions need to be tested for activity concentration. The present work explores the radionuclide concentration and the radon exhalation of bricks obtained recycling different types of potentially radioactive wastes: i) trachyte as by-product resulting from quarrying operations, and ii) two different

types of industrial sludge derived from ceramic tiles industry. Raw materials were studied to foresee any potential radioactive risk derived from their use as secondary raw materials, while bricks were investigated to assess the influence of mineralogy and texture on their radioactive properties and their effective radon-risk. The results obtained here show that, although radon emanation in bricks is primarily determined by radionuclide concentration in the raw materials, textural features significantly affect radon mobility and exhalation.

Key words: Bricks; Radioactivity; Radon; Building materials; Industrial by-products.

## Introduction

Building materials produced from rocks and sediments (clay, sand, gravel and soils) contain natural radioactive elements at highly variable concentration levels and can constitute Naturally Occurring Radioactive Materials (NORM) [1-11]. Natural radioactivity of building materials contributes to the mean annual radiation dose to population both in terms of external irradiation directly emitted from the material and of internal exposure related to the radon exhaled [12-14]. External radiation exposure is determined by direct gamma radiation from external sources, and can be assessed from the activity concentrations of radium ($^{226}$Ra), thorium ($^{232}$Th), and potassium ($^{40}$K). Internal radiation exposure by building materials. is caused by inhalation of gaseous radon, released from pores and fractures in the material itself [15-17]. NORM in building materials are mainly associated with the radioactive families of $^{238}$U, $^{232}$Th, and the primordial $^{40}$K, the radioactivity from the $^{235}$U family being negligible as compared to $^{238}$U on the basis of their relative isotopic abundance. Particular attention should be paid to radon ($^{222}$Rn), thoron ($^{220}$Rn), and their daughters, whose inhalation enhances the risk of bronchial and lung cancer [18,19]. NORM include several materials such as bulk rocks used as dimension stones, whose radioactivity is tightly connected with their petrography, or bricks, tiles, cement, concrete and other materials manufactured from mixtures of geological materials such as

clay, sand, gravel and other components from local or remote sources. Activity concentration of these components will contribute to the average radioactivity of the final building material.

In the last decades, the amounts of waste from human activities and by-products from the industry has been constantly increasing, affecting disposal costs and rising dramatic environmental concerns. In addition, our society is facing a progressive shortage of geo-resources as virgin raw materials. Thus, industry searches for alternative secondary raw materials, including the recycling of both wastes and by-products. This trend is partly motivated by an increasing awareness of the need for green strategies [20-28], and partly by the perspective of reducing costs, especially in the production of building material. Although mitigating the impact on the environment by reducing primary geo-resources exploitation, and often even improving their properties, these products are required to undergo health risk assessment and fulfil health standards before being commercialised [14,29,30]. When waste and by-products are incorporated into a newly designed building material, the final product will contain all their original chemical components, including radionuclides, yielding a mixture of stable and radioactive components depending on the amounts and composition of the precursor materials employed [31]. Moreover, the texture of the final product may also change during the production process, therefore modifying the permeability of the final product to gases. For example, mineralogy and pore structure of bricks may significantly change during firing, depending on the different raw materials used [32]. Building materials containing secondary raw materials may potentially expose people to radiation: for this reason, it is necessary to investigate radioactivity on both raw materials and final products [33].

In Europe, the first attempt to regulate radioactivity of building materials dates back to 1999, when the European Commission released the Radiation Protection 112 [12], a document containing criteria and application rules for dose assessment. In order to estimate exposure from building materials, Radiation Protection 112 introduced the index I, calculated from $^{226}Ra$, $^{232}Th$ and $^{40}K$ activity concentrations experimentally determined by high resolution gamma spectrometry. However, it is

only in 2014 that the European Union enforced the previous documents into the Council Directive 2013/59/Euratom [34].

Radiation Protection 112 guidance [12] mandates that "*when industrial by-products are incorporated in building materials and there is reason to suspect that these contain enhanced levels of natural radionuclides, the activity concentrations of these nuclides in the final product should be measured or assessed reliably from the activities of all component materials".* Article 75 of the Council Directive 2013/59/Euratom [34] encompasses different types of building materials, dividing them into natural materials and materials incorporating residues from processing industries. If the activity concentration index (I) of these residues are below the reference levels imposed by the Council Directive 2013/59/Euratom [34], the derived building materials can be used without restriction.

In view of a safe re-use in bricks of by-products potentially enriched in natural radioactivity, their physical, chemical, mineralogical, and radiological properties should be considered and accurately characterised. The Council Directive 2013/59/Euratom [34] does not provide guidelines to account for the specific radon exhalation/emanation contribution from the building materials. This specific issue has been recently reviewed in detail by the COST Action Tu1301 NORM4BUILDING, that contributed to collect and organize available information, and set up operational guidelines for the management of all building materials including those containing NORM by-products, and for the formulation of new synthetic ones [14,33]. Radiological aspects in the recycling of by-products in the manufacturing of cement, concrete, ceramics, and other construction materials are discussed in Chapter VII of the COST Action Tu1301 NORM4BUILDING [33]. On the contrary, both traditional bricks and bricks produced using NORM by-products have been poorly studied and most of the standards that regulate radioactivity [12, 34] addressed gamma radiation rather than radon exhalation and the related control of texture and porosity.

In this work, we describe the results of an integrated approach aimed at characterizing radioactivity and mineralogy of two series of newly designed bricks obtained from the same base clays, tempered with two different types of ceramic sludge and a by-product of quarrying activity, consisting of finely

fragmented trachyte waste. Both these types of industrial by-products may potentially increase radioactivity of the bricks: sludge from ceramic production could contain radioactive elements derived from the additives used for specific treatments (e.g. sintering, hardening, whitening) or added to glaze, such as zircon [36]; trachyte is a volcanic rock characterised by relatively high concentrations of radionuclides [37].

The paper is organised as follows:

- determination of the radioactivity level of bricks as well as of the single raw materials used such as base clay and temper from industrial by-products;
- correlation of radioactivity with mineralogical and physical features, to predict radioactivity in newly designed building materials when produced using potentially radioactive by-products;
- comparison of the radioactivity and the mineralogy of a set of conventional bricks, the mineralogy, texture and mechanical properties of which had been already previously determined [27,30,32,35], with the radioactivity and mineralogy of these new products.

## 2. Materials

A set of different bricks, and corresponding raw materials, have been analysed. Raw materials include four different types of clay, tailings from quarrying activity, two types of sludge from ceramic industry, and a dye additive (Table 1). The following clay raw materials provided by the Company San Marco-Terreal (Italy) were considered: LG (*Laminato Giallo*, i.e. "Yellow Laminated"), LRS (*Laminato Rosa*, "Pink Laminated"), LRSS (*Laminato Rosso*, "Red Laminated") and LRSSF (*Laminato Rosso Forte*, "Intense Red Laminated"). These clays have similar mineralogy but different relative abundance of their components, especially carbonates [27]. Two types of industrial by-products replacing the traditional temper to produce experimental bricks were characterized: i) two types of sludge derived from ceramic industry (samples F and PIR) [35]; ii) a finely fragmented trachyte waste produced by quarrying activity (sample TR) at M. Altore, in the Euganean Hills

Volcanic District (north-eastern Italy) [30]. Furthermore, a Mn-oxide-based dye additive was also considered (sample MN), as it is used in one of the commercial bricks here studied (sample N).

The bricks analysed can be grouped in three different categories (Table 1): i) commercial bricks (produced by San Marco-Terreal); ii) experimental bricks obtained by adding the trachyte waste; iii) experimental bricks obtained by adding the two types of sludge from ceramic industry.

The six commercial bricks (samples GP, N, RS, RSS, R6, RCF) are produced by adding 10 wt. % of a quartz-rich sand (sample SS) to the different clayey materials (LG, LRS, LRSS, LRSSF) (Table 1). The mixtures are fired at different temperatures (Table 1), depending on the specific clay used. In addition, different proportions of a dye (additive MN) were added to sample N, up to 15 wt. %.

Nine experimental bricks were obtained by tempering the most siliceous clayey material (LRSSF) with 5, 10 and 15 wt. % (samples with prefix B5, B10 and B15, respectively) of sand-sized fragments of trachyte, and firing each mixture at three different temperatures: 900, 1000, 1100 °C (suffix 9, 10 and 11, respectively).

Two additional experimental bricks (samples MF and B_PIR) were obtained tempering the most carbonate-rich clay (LGP) with 10 wt. % of the two different types of sludge (F and PIR); both mixtures were then fired at 1050 °C (same firing temperature as commercial bricks GP and N obtained from the same base clay). Types of material and experimental conditions are summarized in Table 1.

## 3. Methods

The chemical composition of the samples was determined by X-ray fluorescence (XRF) on an S4 Pioneer (Bruker AXS) spectrometer, with an estimated detection limit of 0.01 wt. % for major elements; trace elements, expressed in ppm, have the following analytical detection limits: Zr = 15 ppm, Rb = 18 ppm; Sr = 20 ppm; Cr 11 = ppm; Zn = 15 ppm; Ni = 1 ppm; Pb = 17 ppm. ZAF method was employed for quantitative analysis [38], while the NCS DC 74301 (GSMS-1) standard was used for calibration [39].

X-ray powder diffraction (XRPD) was applied to identify the mineral phases of raw materials and fired products. Diffraction data were acquired using a PANalytical X'Pert PRO diffractometer, operating in Bragg-Brentano reflection geometry with CoKα radiation, 40 kV of voltage and 40 mA of filament current, equipped with an X'Celerator detector. Qualitative analysis of diffraction data was carried out with X'Pert HighScore Plus® software (PANalytical) and the PDF-2 database. The petrographic and textural characteristics of thin sections were examined under a polarized light optical microscope (Olympus DX-50, equipped with a Nikon D7000 digital microphotography system).

Texture and reaction microstructures were examined by Scanning Electron Microscopy (SEM) with a CamScan MX-2500 microscope, coupled with an EDAX Sapphire Si(Li) detector (LEAP+Si(Li) crystal), equipped with a $LaB_6$ cathode operating at 20 kV and 160 nA.

The distribution of pore-access size (radius range: 0.001-100 μm) was determined by Mercury Intrusion Porosimetry (MIP) on a Model 9410 Micromeritics Autopore apparatus, which can generate a pressure of 414 MPa. Freshly cut samples of approximately 2 $cm^3$ were oven-dried for 24 hours at 110 °C and then analyses.

Nitrogen adsorption was used to determine brick porosity in the range (in diameter) between 0.0002 and 0.3 μm. Sorption isotherms were obtained at 77 K, on a Micromeritics Tristar 3000 in continuous adsorption conditions. Prior to measurement, samples were heated at 130 °C for 24 h and outgassed to $10^{-3}$ Torr on a Micromeritics Flowprep. Specific surface area of pores was determined by Brunauer–Emmett–Teller (BET) theory based on the physical adsorption of gas onto the surface of a solid.

Activity levels of raw material and finite products were evaluated both measuring concentrations of K, U, Th and descendants by XRF, and high-resolution γ-ray spectroscopy. Samples were analysed with two p-type coaxial Hyper Pure Germanium crystal detectors (HPGe), a PROFILE (Ortec-Ametek Inc.) with an extended energy range (20–2000 keV) and a conventional GEM model (Ortec-Ametek Inc.) with an energy range 80-2000 keV. These detectors have relative efficiency of 20% and 38%, and resolution (FWHM) at 1332.5 keV of 1.9 keV and 1.8 keV, respectively. Both systems

were calibrated for energy and efficiency using a liquid standard source (Eckert & Ziegler Multinuclide standard solution 7501) in a jar geometry (diameter = 56 mm; thickness = 10 mm). Spectra were acquired for 1 day to optimize peak analysis. Spectra were subsequently processed and analysed with the Gamma Vision-32 software (version 6.07, Ortec-Ametek Inc.) [40]. $^{226}$Ra was determined at 186 KeV correcting the peak area by the $^{235}$U interference according to the method proposed by Gilmore (2008) [41], under the hypotheses of secular equilibrium between $^{226}$Ra-$^{238}$U and natural $^{235}$U/$^{238}$U isotopic ratio. $^{238}$U and $^{232}$Th were then determined using the emissions of their radioactive daughters $^{226}$Ra and $^{228}$Ac.

The minimum detectable activity ($CR_{MDA}$) was calculated according the so-called Traditional ORTEC method available in GammaVision according to the expression:

$$CR_{MDA} = \frac{\frac{100}{SENS} \cdot \left( \sqrt{2 \cdot B_1 + \frac{2500}{SENS^2}} + \frac{50}{SENS} \right)}{LT}$$

where SENS is the Peak Cutoff value (%) on the Analysis tab (40% in this work), B1 is the Peak background, and LT is the Live Time (sec).

Conversion from activity concentration (Bq/kg) to bulk elemental weight fraction was obtained through the following conversion factors [42]:

1% K = 309.7 Bq/kg

1 ppm U = 12.35 Bq/kg

1 ppm Th = 4.072 Bq/kg

Council Directive 2013/59/Euratom [34] defines the Activity Concentration Index (I) in order to quantify and regulate the exposure to gamma radiation originating from radionuclides in building materials:

$I = C_{Ra226}$ /300 Bq/kg + $C_{Th232}$ /200 Bq/kg + $C_{K40}$ /3000 Bq/kg

where $C_{Ra}$, $C_{Th}$ and $C_K$ are the specific activities of $^{226}$Ra, $^{232}$Th and $^{40}$K, respectively, expressed in Bq/kg. The activity concentration index value of 1 can be used as a conservative screening tool for identifying materials that may cause the reference level (1 mSv per year) to be exceeded [34].

The alpha-index (Iα) may be used to regulate the exposure to radon originating from radionuclides in building materials [43,44]:

$I\alpha = C_{Ra}/200$ Bq/kg

The reference levels of Iα and I are 0.5 and 1, respectively [12,34,43].

To assess the radiation hazard of the bricks, the radium equivalent activity (Ra_eq) was calculated according to the method introduced by Beretka and Methew (1985) [45] with the following equation:

$Ra\_eq = C_{Ra} + 1.43\ C_{Th} + 0.07\ C_K \leq 370$ Bq/kg.

Radon emanation and exhalation from a porous material in indoor air should be regarded as a combination of different processes and factors. Firstly, the radon emanation derives from the solid-phase lithology and its characteristic naturally occurring radioactivity. Secondly, since radon atoms recoil and migrate into the pore space, texture and physical features can sensibly affect exhalation.

Radon exhalation from the investigated materials was measured by electrets. To this scope, brick samples were cut into cubes (edge = 5 cm) to obtain a measurable external surface. Each sample was introduced in suitable airtight bottles (volume = 0.00372 $m^3$) containing two electrets in SST configuration [Kotrappa]; prior to analysis, radon blank was checked in the closed bottle in the absence of sample. For each sample a parallel measurement with an empty bottle was carried out for background radon subtraction under the same environmental conditions. After tightly sealing the bottles, radon exhalation was allowed over a suitable time (5-7 days); eventually the bottles were opened and electrets retrieved and read, and the experiment repeated. The final exhalation value was taken as the average of two subsequent readings. The radon exhalation rate ($Q_A$) was then evaluated as follows:

$$Q_A\ \left[\frac{Bq}{d}\right] = \frac{V\lambda}{1 - \frac{1 - e^{-\lambda T}}{\lambda T}}\left[\langle C\rangle_{sample} - \langle C\rangle_{blank}\right]$$

where λ is the decay constant of $^{222}Rn$ (0.18145 $d^{-1}$), $T$ the measurement time in days, $V$ the free volume inside the bottle, $C$ the radon concentration in Bq/$m^3$ and the angular brackets indicate average over time ($T$).

Finally, specific surface exhalation rate (*Ea)* is calculated dividing $Q_A$ by the sample surface *S* in square meters:

$$Ea\ \left[\frac{Bq}{d\ m^2}\right] = \frac{Q_A}{S}.$$

The radon release per unit mass of the material, specific mass exhalation rate (*Em*), can be calculated dividing $Q_A$ by the mass *m* in kilograms of the sample:

$$Em\ \left[\frac{Bq}{d\ kg}\right] = \frac{Q_A}{m}.$$

According to Stoulos et al. (2003) [13] and Righi and Bruzzi (2006) [44], the radon emanation coefficient (η), representing the percentage of radon produced from grains and free in porous system, can be also defined as follows:

$$\eta = Q_A / C_{Ra}\ m\ \lambda_{Rn}$$

where $Q_A$ is the measured radon exhalation rate (Bq/d), $C_{Ra}$ the $^{226}Ra$ content (Bq/kg), $\lambda_{Rn}$ the $^{222}Rn$ decay constant (1/d), and *m* is the mass of the sample (kg).

Data obtained from the previously described analytical methods, were statistically treated according to multivariate approaches, consisting in the cluster analysis (CA) and principal component analysis (PCA), using Statgraphics® Centurion XVI software package. CA represents an optimal approach for the management of chemical data, since it can describe the natural structure of the dataset and homogeneous subsets of samples (defined as clusters), which differ from the others to some extent, expressed by the dissimilarity level. PCA is a multivariate approach which converts a dataset originally described by numerous variables, possibly correlated, into a dataset expressed new variables (called principal components), which emphasises the maximum variability among the samples. PCA was performed on the chemical data to evaluate the elements mainly affecting the differences between bricks, and it was also applied considering the physical parameters (density, porosity, surface area) as well as the those related to the radiation activity (I, Iα, Ea, Em, $C_{Ra}$) in order to define which of these variables manly contribute to describe the differences among the bricks, and to identify possible correlations between various parameters. These statistical approaches, therefore,

were used to better interpret the possible relationships between the physical, compositional and structural parameters of the bricks with a special attention to the radon-related effects.

## 4. Results

### 4.1 Raw materials

#### *4.1.1 Chemical and mineralogical characterization*

Chemical composition of clayey materials shows significant differences in CaO and MgO suggesting variable content in carbonates (see Table 2). In particular, samples LRS and LG have both higher concentrations of these oxides and Loss on Ignition (LOI) than LRSS and LRSSF. This agrees with the mineralogical composition (Table 3) which indicates that they are illite-chlorite carbonate-rich clays, with significant amounts of calcite and dolomite.

Trachyte (sample TR) is rich in $Na_2O$ and $K_2O$ (Table 2; $Na_2O + K_2O \sim 10$ wt. %), consistently with the abundance of anorthoclase (an alkali feldspar) and plagioclase, associated with minor amounts of biotite and quartz (Table 3) (see Coletti et al., 2018 [30], and also data referring to M. Altore trachyte in Germinario et al., 2018 [46]); zircon and magnetite occur as accessory minerals as recognised under optical microscope, and account for the Zr (559 ppm) and $Fe_2O_3$ (3.26%) contents (Table 2).

Sludge materials F and PIR are rich in silica and alumina (Table 2). Quartz and feldspar dominate their mineralogy (Table 3). Sludge F is characterized by mullite and amorphous phase (Table 3) [35], suggesting an origin from ceramic production in which the firing process reached temperatures above 900 °C, when mullite starts to form from illite-muscovite and/or kaolinite breakdown [47] and sintering occurs. Sludge PIR contains higher amounts of feldspars (both alkali-feldspar and plagioclase), illite and minor amounts of carbonates, as evidenced by the content in CaO and from LOI (2.19 and 4.35 wt. %, respectively; Table 2), and by the presence of calcite reflections in the diffraction pattern (Fig. 1S). This sample also contains relatively high amounts of Zn, Cr and Sr (4915, 2201 and 567 ppm, respectively). These elements are diagnostic of ceramic manufacturing applied to confer specific physical and aesthetical characteristics to the final material body and

surface: in particular, ZnO is generally used in ceramics as a fluxing agent, Cr to obtain a wide variety of different hues, while Sr produces matte glazes [48]. The high amount of Zr both in sludge F and PIR (1583 and 7157 ppm, respectively) is probably related to the wide use of this element in the ceramic industry both for tile enamel whitening and as a structural component; however, its use has been strongly reduced in recent times, to avoid its excessive concentration in NORM [48]. PIR presents also moderate amounts of Pb (77 ppm). In the past, Pb has been used as melting agent; nowadays it is mainly used in the production of glaze.

Sample MN is a Mn-oxide ($Mn_2O_3$; hausmannite) and is used as a dye (added to the raw materials in ~15 wt. %) to obtain dark-grey coloured bricks [27].

### *4.1.2 Natural radioactivity*

Table 4 reports the activity concentration of $^{226}Ra$, $^{232}Th$ and $^{40}K$ in the raw materials. The measured values on clay span over a range between 29 Bq/kg and 50 Bq/kg for $^{226}Ra$, between 34 Bq/kg and 59 Bq/kg for $^{232}Th$, and between 29 Bq/kg and 50 Bq/kg for $^{40}K$. These values are consequently reflected in the correlated I value (Table 4), providing a minimum of 0.47 for clay LG and a maximum of 0.70 for clay LRSS, in both cases below the recommended value of 1 [34].

Also, α-indexes of clayey materials have all values below the recommended value ($I\alpha \leqslant 0.5$, Table 4) [12], with the maximum value registered for clay LRSS ($I\alpha = 0.25$).

Among the industrial by-products, F shows very low $^{226}Ra$ activity concentration with values below the minimum detectable activity of the instrument, while TR and PIR have the highest measured values. TR has 52 Bq/kg of $^{226}Ra$ and shows a very high value of $^{40}K$ (1210 Bq/kg), approximately twice as much as the other samples, owing to the abundance of alkali feldspars in trachyte (Table 3), which is naturally characterised by a relatively high radioactivity [37].

Sludge PIR has the highest activity concentration value of $^{226}Ra$ (120 Bq/kg, Table 4), responsible for the high Iα value (0.60, Table 4), probably connected to the high content in Zr, and supposedly in other high-field-strength elements (HFSE) such as U and Th [49]. Dye additive MN has very low

values of activity concentration (Table 4), below minimum detectable activity for all the analysed elements. The highest Ra_eq have been detected for samples TR and PIR (216 Bq/kg and 219 Bq/kg, respectively), much higher than those of the clayey materials, quartz-rich sand, and of the other by-products, with values between 30 Bq/kg and 189 Bq/kg (Table 4). This is in agreement with activity concentration of the critical radionuclides in the different raw materials, determining slightly higher concentration levels than average NORM.

## 4.2 Bricks

### *4.2.1 Chemical composition and mineralogy*

The chemical composition of the investigated bricks (Table 2) is consistent with that of the clay materials used and the temper added (Table 1). The dendrogram of figure 1a reports the hierarchical cluster analysis of the chemical composition performed on XRF data (Table 2). It shows that bricks GP and FM produced using a carbonate-rich clay (LG) are clustered together (cluster 1) and separated from the two bricks N and B_PIR produced using the same clay, but obtained by adding the by-products MN and PIR, respectively, which appear as isolated outliers (Fig. 1a) for the higher MnO, Zr and Zn contents, respectively (score and loading plot in Fig. 1b, Table 2). Bricks obtained using low-Ca clays (LRSS and LRS) form a distinct cluster (cluster 2) (Fig. 1a), whereas those produced using clay LRSSF group all together in cluster 3 (Fig. 1a). These latter were obtained adding to the base clay a quartz or trachyte sand, respectively; despite the different chemical composition of the added temper, these bricks group together and are separated from all the others for the higher content in $SiO_2$, $Na_2O$, $Fe_2O_3$, $P_2O_5$ as well as of Ni.

From a mineralogical point of view, the commercial bricks can be distinguished on the basis of the used clayey materials, temper/additive and firing temperature (Table 3). The new minerals formed at temperature above 800 °C are the result of carbonates (calcite and dolomite) and illite decomposition and their sub-solidus reactions with quartz and feldspar grains. These phases form reaction rims and

often display non-stoichiometric compositions. Nonetheless, the main reactions taking place at the grain boundaries can be described as follows [22,23,50]:

$$2\ CaCO_{3(calcite)} + 0.4\ KAl_4Si_7O_{20}(OH)_{4(illite)} \xrightarrow{800\text{-}850\ ^\circ C} 0.6\ Ca_2Al_2SiO_{7(gehlenite)} + 0.4\ KAlSi_3O_{8(sanidine)} + 1.6\ H_2O + 1.2\ CO_2$$

$$CaCO_{3(calcite)} + SiO_{2(quartz)} \xrightarrow{>900\ ^\circ C} CaSiO_{3(wollastonite)} + CO_2$$

$$CaMg(CO_3)_{2\ (dolomite)} + 2\ SiO_{2(quartz)} \xrightarrow{>900\ ^\circ C} CaMgSi_2O_{6(diopside)} + 2\ CO_2$$

Brick N contains bustamite $CaMnSi_2O_6$, a member of the wollastonite group, isomorphic with wollastonite, which developed from the sub-solidus reaction between hausmannite, calcite and quartz [35]:

$$CaCO_{3(calcite)} + 2SiO_{2(quartz)} + Mn_2O_{4(hausmannite)} \xrightarrow{>900\ ^\circ C} CaMnSi_2O_{6(bustamite)} + Mn_2O_3 + CO_2$$

Brick R6, instead, shows a completely different mineralogy, characterised by persistence of clay-forming minerals such as illite, chlorite, and still showing carbonates (calcite and dolomite) because fired at 600 °C, thus below their breakdown temperature [27,47,51] (Table 3).

Bricks obtained from the addition of the two types of sludge (F and B_PIR) are very similar under a mineralogical viewpoint to the commercial brick GP, also manufactured using the same carbonate-rich clay LG (Table 3), being all enriched in wollastonite and diopside.

All the experimental bricks obtained by adding trachyte waste to the LRSSF clay display similar mineralogical composition, with the occurrence of newly formed silicate phases. Diopside is present in small amounts, being the raw clay (LRSSF) very poor in dolomite, while gehlenite is abundant and its amount increases as a function of increasing firing temperatures (Table 3). Although firing temperatures always exceed typical dolomite and calcite decarbonation temperatures (750 and 850 °C, respectively), small amounts of calcite survived decomposition as shown in the diffraction patterns of the bricks fired at 900 and 1000 °C, while dolomite completely disappeared. Moreover, the small amount of illite observed in bricks fired at 1000 °C indicates that amorphisation was not

complete at this temperature. This may also be connected to inhomogeneity in the temperature distribution within the kiln, which could have determined the survival of structural domains of minerals generally destructured at slightly lower temperatures than firing temperature [30] or as consequence of non-total amorphisation of illite. Furthermore, biotite in these bricks derives from the trachyte waste; its abundance gradually decreases with increasing firing temperature (Table 3).

### *4.2.2 Radionuclides activity concentration*

The radioactivity levels measured in the studied bricks are comparable with those reported in the literature [5,7,13,52,53,54]. The lowest $^{226}$Ra value was measured in brick N, equal to 29 Bq/kg (Table 4). This value is lower than that measured in the clay GP used to produce this brick (45 Bq/kg). This can be explained assuming a dilution effect due to the addition of the dye additive MN, which presents the lowest concentration of natural nuclide among the studied materials (Table 4). The same effect can be invoked when the sludge F (Table 4) is added to the same clayey material LG. Radionuclide concentration in the brick FM results to be lower (40 Bq/kg) than that of the brick obtained using the same clay but tempered with standard quartz-rich sand SS (brick GP, 45 Bq/kg). Conversely, the brick B_PIR, obtained from the same clay LG with the addition of the sludge PIR, characterised by a high radioactive concentration (120 Bq/kg), displays higher $^{226}$Ra concentration (55 Bq/kg) than brick GP (Table 4). The same considerations apply to $^{232}$Th and $^{40}$K concentrations. Bricks tempered with the trachyte waste TR present generally higher radioactive concentration than the corresponding commercial bricks obtained using the same clay tempered with a quartz-rich sand (brick RCF, 43 Bq/kg). Bricks tempered with trachyte waste have values of $^{226}$Ra concentration between 46 and 55 Bq/kg, while $^{232}$Th concentration ranges between 43 and 56 Bq/kg, except for bricks B5.9 and B15.11, in which it is 66 Bq/kg. $^{40}$K concentration for this set of bricks is comprised between ~ 600 and 1016 Bq/kg, and the maximum values have been measured for bricks B5.9 (1016 Bq/kg), B5.11 and B15.11 (1000 Bq/kg).

The activity indexes (Table 4) range between 0.53 and 0.82 for I and 0.15 and 0.27 for Iα, respectively. None of the two parameters exceeds the reference levels reported in the Council Directive 2013/59/Euratom [34] and RP112 [12]. The radium equivalent activity (Ra_eq) is always < 370 Bq/kg.

### *4.2.3 Radon exhalation rate*

In order to determine the contribution of the by-products to the internal radiation dose, which accounts for the largest fraction of radiation dose from building materials, $^{222}Rn$ emission of the investigated bricks was measured. Table 5 lists the radon exhalation rates and emanation fraction. Among the commercial bricks analysed, the lowest radon exhalation rate has been recorded for brick RCF (Table 5), produced using the clay material (LRSSF) with the lowest carbonate content (see CaO wt. % in Table 2). The bricks produced with clays richer in carbonates show wide variability. All the bricks produced with the clay LG, enriched in carbonates, and tempered with different materials (bricks GP, N, FM and B_PIR) show considerable differences in their exhalation rate. This is undoubtedly partially determined by differences in the chemical composition of the temper (e.g. bricks FM and B_PIR made using the two different types of ceramic sludge), partially by the textural features, especially porosity, which develops during firing upon $CO_2$ release from calcinated carbonates, and depending on the different reactions taking place at increasing temperature and on the specific temper used. This is particularly evident when considering the two bricks RSS and R6, both based on clay LRSS and the same quartz-rich temper but displaying significantly different $^{222}Rn$ exhalation rate (0.017 Bq/d and 0.084 Bq/d, respectively). In these two materials, the different firing temperatures (950 °C for RSS vs. 600 °C for R6) determined the development of significantly different textures, in terms of both pore-size distribution and pore fraction [35]. Since $^{226}Ra$, the precursor of $^{222}Rn$, has the same concentration in both bricks (Table 4), the high radon exhalation rate observed in brick R6 (Table 5), is reasonably determined by the different pore structure. The same stands for the lower

surface exhalation rate of brick RSS (2.84 Bq/d·m$^2$) as compared to brick R6 (8.58 Bq/d·m$^2$) (Table 5).

Bricks obtained using trachyte waste as a temper have generally higher exhalation rate when fired at lower temperature (e.g. 900 °C). Moreover, radon exhalation rate decreases increasing the amount of trachyte waste added (Table 5). This is apparently a contradiction, considering that trachyte has significantly higher NORM level than clay (Table 4). However, this could be attributed to the influence of trachyte acting as a flux agent capable to modify the matrix texture [30] and promote sintering at lower firing temperature than other types of temper. These textural changes thus reduce radon exhalation rate despite the higher precursor activity concentration levels [55].

Bricks produced with addition of sludge (FM and B_PIR) have intermediate values of surface exhalation rate (2.84 Bq/d·m$^2$ and 2.23 Bq/d·m$^2$, respectively).

### *4.2.4 Density and porosity*

Bricks (GP, N, FM, B_PIR and RS) obtained using a carbonate-rich clay (LG and LRS) yielded the highest values of open porosity ε (%), ranging between 42 and 50% (Table 6). Among the bricks produced using sludge (F and PIR), B_PIR is the one showing the lowest ε value: sludge PIR caused a decrease in total porosity of about 6% with respect to the commercial brick GP (produced using the same clay, and tempered with quartz-rich sand). It is also interesting to observe the effect of this sludge on brick microstructure. Bricks display higher average pore size, as shown by comparing the percentage of pores larger than 1 μm in commercial bricks and in those produced with sludge (Table 6). Brick FM, produced using sludge F, has a higher open porosity (50%), mainly constituted by pores smaller than 1 μm ($\varepsilon_{<1\mu m}$ = 47%). Nonetheless, brick FM presents the highest density (1600 kg/m$^3$, Table 6) among the bricks produced with the carbonate-rich clay LG. This could be determined by the specific properties of sludge F (Table 3) rich in amorphous phase, as revealed from the XRPD data and for the highest melting phase reached during firing, capable to seal pores.

Commercial bricks (RSS, R6 and RCF) produced using carbonate-poor clays (LRSS and LRSSF) display lower open porosity (between 34% and 39%, Table 6), with brick R6 showing the lowest value, being fired at low temperature (600 °C). This brick has an apparent density ($\rho_a$ = 1700 kg/m$^3$) considerably different from the actual density ($\rho_r$ = 2580 kg/m$^3$), suggesting a high fraction of closed pores. Nevertheless, small size open pores remain predominant, as confirmed by the high value of adsorbed nitrogen leading to a specific area of 10.24 m$^2$/g according to the BET method, i.e. the highest micro-porosity value among all the other samples (Table 6).

Open porosity in bricks obtained by adding trachyte waste is quite variable but shows a general trend: it increases in bricks fired at 1000 °C and decreases in those fired at 1100 °C, while bulk density ($\rho_r$) increases with the firing temperature. Evaluating the pore range < 0.1 μm, small pores prevail in bricks fired at 900 °C; their fraction gradually decreases with increasing firing temperature and with increasing trachyte waste content, also when compared with brick RCF obtained using the same clay, but different temper. Thus, the addition of trachyte tailings in the experimental bricks is likely responsible of changes in the microstructure, enhancing bulk density and pore size, leading to the formation of a more compact material [30]. Changes in the pore system are also well demonstrated by the decrease of the specific surface area at increasing firing temperature, as confirmed by the BET experiment (Table 6).

## 5. Discussion

The obtained emanation coefficients range between 0.002 and 0.109 (Table 5) in agreement with those reported by Stoulos et al. (2003) [13] and Righi and Bruzzi (2006) [44]. Most of the bricks have η value below 0.04, with the exception of brick R6 reaching 0.109; this result is related to the material texture and porosity [4,56,57,58], despite the radionuclide concentration being similar to that observed for the other bricks (Table 4).

The main parameters describing radon release from a solid are the radon surface exhalation rate *Ea* (Bq/d·m$^2$), and the radon mass exhalation rate *Em* (Bq/d·kg). These values can be either obtained

from direct measurements [56] or estimated when other parameters of the materials are known [58,59], i.e. the $^{226}$Ra activity concentration ($C_{Ra}$, Bq/kg), the coefficient of emanation (η), the porosity (ε, %) and the density (ρ, kg/m$^3$). Nonetheless, there are limitations in both these approaches. Previous works describe porosity as a key factor controlling emanation power of building materials [13,56], but without quantifying its actual effect. Indeed, porosity plays an important role in physical-mechanical properties and in the decay behaviour of building materials [27,60,61,62], and so it does for radon migration [63,64]. Moreover, chemical and mineralogical composition and texture of bricks may change considerably, depending on the starting raw materials, their relative abundance and grain-size, and firing conditions [27,35]. Therefore, they represent ideal model materials wherein to investigate the influence of porosity on radon exhalation. In general, assessment of radon emanation power requires better understanding on the influence of porosity and pore-size distribution, and on the influence of radionuclides concentration in relation to texture, which determines the emanation pathways ultimately determining the effective amount of radon emitted.

Semkow and Parekh (1990) [65] described the importance of grain-size, which controls radon diffusion through porosity and surface area [66].

Mass emanation (*Em*) normalised to porosity ($Em_\varepsilon$) can be obtained by the following equation:

$$Em_\varepsilon = 1 - Em\ (\varepsilon - C_{Ra}) / C_{Ra}$$

and mass emanation normalised to $^{226}$Ra concentration ($Em_{CRa}$) as:

$$Em_{CRa} = 1 - Em\ (C_{Ra} - \varepsilon) / \varepsilon,$$

where *Em* is the measured mass exhalation rate (Bq/d kg), $C_{Ra}$ the $^{226}$Ra activity concentration (Bq/kg), and ε the porosity (%).

The binary plot of radon exhalation rate vs. normalised mass emanation clearly shows a better correlation when data are normalised to porosity ($Em_\varepsilon$; $R^2 = 0.96$; Fig. 2a) than to $^{226}$Ra concentration ($Em_{CRa}$; $R^2 = 0.86$; Fig. 2b). This suggests that texture, and especially open porosity, affects radon exhalation more than $^{226}$Ra concentration.

According to Semkow and Parekh (1990) [65], radon emanation power is sensitive to pores with size between $5 \cdot 10^{-40}$ μm and 0.1 μm, although the latter are a key for radon transport inside the material. This is confirmed by the data collected on bricks in the present study. The correlation between emanation mass (*Em*) measured by E-PERM and total porosity as measured by MIP (Fig. 3a) is very poor ($R^2 = 0.03$), while the one with the fraction of pores < 0.1 μm (Fig. 3b) is considerably better ($R^2 = 0.59$). This suggests that the fraction of smaller pores is the most reactive to radon emission. The same behaviour is observed considering the specific surface areas, $S_0$. The specific surface area can be calculated from the average pore radium *r* (assuming all pores are cylindrical) [35,67], and the total pore intrusion volume dV/V (measured by MIP) as follows:

$$S_0 = 2\pi r h$$

where the average height (*h*) is calculate as:

$$h = \frac{dV^2}{V} / \pi r$$

The correlation between radon emanation mass and specific surface area ($m^2/g$) is much higher ($R^2 = 0.60$; Fig. 3c) than considering the total porosity (Fig. 3a). This is related to a linear relationship between emanation power and the specific surface area [68]. This observation is supported also by the data obtained from BET, wherein pores with diameter below 0.3 μm are analysed, although radon mass emanation and BET surface areas correlation is not so straightforward ($R^2 = 0.48$; Fig. 3d).

A similar result was obtained comparing radon emanation mass with the specific surface area $S_0$ assuming the average pore size equal to 0.005 μm and determining *h* by partial dV/V calculated in the range of pores less than 0.005 μm: $R^2$ value obtained in such condition (0.39, Fig. 3e), is similar to what obtained by BET (0.48, Fig. 3d). Thus, despite different analytical methods for the determination of the pores system are considered, the specific surface area is in such case related to a range of pores size overlapping in MIP and BET. According to Semkow and Parekh (1990) [65], the emanation power is less sensitive to larger pores. This is also observed for the studied bricks; when the specific surface area is calculated over the total porosity using an average pore size of 0.5 μm (Fig. 3f), the parameters are not correlated ($R^2 = 0.04$).

Principal Component Analysis (PCA) (Fig. 4a) applied to the main physical properties and chemical components of the bricks further indicates the correlations among textural features, chemistry and radioactivity. The purpose of this analysis is to determine which of these variables is mostly affecting radon emanation of the bricks. The score and loading plot of the first three components (Fig. 4a), shows that PC1 is positively correlated with MnO, CaO and MgO that are grouped with BET surface area ($S_{aBET}$), while it is negatively correlated with variables associated with natural radionuclides activity concentration, bulk density and Fe-oxides. PC2 is positively correlated with variables related to radon exhalation (*Ea* and *Em*), LOI, and fine-size porosity (BET surface area $S_{aBET}$ and $\varepsilon_{MIP<0.1\mu m}$). In order to enlighten differences among the various bricks, the binary plot of PC1 and PC2 was also considered (Fig. 4b). In this case bricks are distributed according to their specific mix design. Thus, bricks obtained from the most siliceous clay (LRSSF) with the addition of trachyte waste are all clustered together as a result of the highest radioactive content, expressed by the values of I, Iα and $C_{Ra}$, the highest bulk density and content of $Al_2O_3$, $Na_2O$, $TiO_2$, $P_2O_3$, Ni, and Rb. On the other hand, bricks obtained from the carbonate-rich clay (LG) are grouped in correspondence to CaO and MgO. Therefore, PCA summarizes the influence of different mineralogical, chemical and physical variables in relation with radon emanation and transport.

## 6. Conclusions

Radioactivity and radon exhalation rate of bricks produced using NORM by-products have been determined and compared with those of similar commercial bricks. All investigated samples provided values below the reference levels indicated in the Council Directive 2013/59/Euratom concerning basic safety standards for protection against exposure to ionising radiations.

While radon emanation in bricks is primarily determined by the concentration of the parent radionuclides from the uranium-238 series in the samples resulting from the composition of the mixture of natural and waste materials, radon exhalation also depends on the pore system, which controls radon mobility. Because the characteristics of the pore system are influenced by the initial

mineral composition and by the transformations taking place during firing process, firing conditions also contribute to determine net radon exhalation rate. Starting from the same clayey material as commercial brick RCF and adding increasing proportions of trachyte waste, we may expect a progressive increase of radon exhalation. Instead, although all the samples produced adding the trachyte waste present higher exhalation rate compared to brick RCF, our data show that radon exhalation rate decreases by increasing the amount of trachyte. This can be explained by considering that the alkali feldspar present in the trachyte waste acts as a flux, thus promoting sintering proportional with trachyte waste content and firing temperature. Total open porosity initially increases from 900 °C to 1000 °C due to proceeding of sheet silicates decomposition, and then decreases from 1000 °C to 1100 °C, due to further sintering, while open porosity < 0.1 μm and surface area (both BET and MIP) continuously decrease with increasing temperature. A similar observation arises considering samples RSS and R6. These two samples have the same composition, but they have been fired at different temperatures (950 °C and 600 °C, respectively). For this reason they have similar $^{226}$Ra, $^{232}$Th and $^{40}$K radioactivity concentration, but significantly different radon exhalation rate, which is four times lower in the sample RSS fired at higher temperature. In this sample, carbonate decomposition and consequent fluxing effect of the released CaO determined an increase in total open porosity, but a significant reduction of open porosity < 0.1 μm and surface area (both BET and MIP), similarly to what observed in samples containing trachyte waste.

This indicates that texture evolution during firing determines significant changes in porosity and pore size distribution, eventually determining changes in gas transport pathways through the pore system and modifying radon exhalation rate.

**Acknowledgments**

This study was funded by Project CPDA134483 of the University of Padova (Raffaele Sassi) and by Junta de Andalucía Research Group RNM179 and by Research Project MAT2016-75889-R

(Giuseppe Cultrone). The authors are grateful to the company *SanMarcoTerreal Italia srl* for collaborating in providing materials and supporting technologies.

## References

[1] M. Al-Jarallah, Radon exhalation from granites used in Saudi Arabia, J. Environ. Radioact. 53 (2001) 91–98.

[2] R. Hewamanna, C.S. Sumithrarachchi, P. Mahawatte, H.C.L. Nanayakkara, H.C. Ratnayake, Natural radioactivity and gamma dose from Sri Lankan clay bricks used in building construction, Appl. Radiat. Isot. 54 (2001) 365–369.

[3] O. Brígido Flores, A. Montalván Estrada, R. Rosa Suárez, J. Tomás Zerquera, A. Hernández Pérez, Natural radionuclide content in building materials and gamma dose rate in dwellings in Cuba, J. Environ. Radioact. 99 (2008) 1834–1837.

[4] J. Chen, N.M. Rahaman, I.A. Atiya, Radon exhalation from building materials for decorative use, J. Environ. Radioact. 101 (2010) 317–322.

[5] N. Damla, U. Cevik, A.I. Kobya, A. Celik, N. Celik, I. Yıldırım, Assessment of natural radioactivity and mass attenuation coefficients of bricks and roofing tile used in Turkey, Radiat. Meas. 46 (2011). 701–708.

[6] H. Kayakökü, Ş. Karatepe, D. Mahmut, Measurements of radioactivity and dose assessments in some building materials in Bitlis, Turkey, Appl. Radiat. Isot. 115 (2016) 172–179.

[7] M. Hegedűs, Z. Sas, E. Tóth-Bodrogi, T. Szántó, J. Somlai, T. Kovács, Radiological characterization of clay mixed red mud in particular as regards its leaching features, J. Environ. Radioact. 162–163 (2016) 1–7.

[8] Y. Raghu, R. Ravisankar, A. Chandrasekaran, P. Vijiayagopal, B. Venkatraman, Assessment of natural radioactivity and radiological hazards in building materials used in the Tiruvannamalai Distric, Tamilnadu, India, using a statistical approach, J. Taibah Univ. Sci. 11 (2017) 523–533.

[9] H. Bártová, J. Kučěra, L. Musílek, T. Trojeck, E. Gregorová, Determination of U, Th and K, in bricks by gamma-ray spectrometry, X-ray fluorescence analysis and neutron activation analysis, Radiat. Phys. Chem. 140 (2017) 161–166.

[10] D. Langimur, Uranium-solution equilibria at low temperatures with applications to sedimentary Ore deposits, Geochim. Cosmochim. Acta 42 (6) (1978) 547–569.

[11] O. Maxwell, H. Wagiran, N. Ibrahim, S.K. Lee, Z. Embong, P.E. Ugwuoke, Natural radioactivity and geological influence on subsurface layers at Kubwa and Gosa area of Abuja, Northcentral Nigeria, J. Radional. Nucl. Ch. 303 (2015) 821–830.

[12] European Commission (1999). Radiation Protection 112, Radiological protection principles concerning the natural radioactivity of building materials, Directorate-General Environment, Nuclear Safety and Civil Protection, Luxembourg ISBN 92-828-8376-0.

[13] S. Stoulos, M. Manolopoulou, C. Papastefanou, Assessment of natural radiation exposure and radon exhalation from building materials in Greece, J. Environ. Radioact. 69 (2003) 225–240

[14] H. Friedmann, C. Nuccetelli, B. Michalik, M. Anagnostakis, G. Xhixha, K. Kovler, G. de With, C. Gascó, W. Schroeyers, R. Trevisi, S. Antropov, A. Tsapalov, C. Kunze, N.P, Petropoulos, Measurement in NORM, Naturally occurring Radioactive Materials in Construction, Integrating Radiation Protection in Reuse, (COST Action Tu1301 Norm4building), Edit by Wouter Schroeyers, Woodhead Publishing (2017) 61–134.

[15] K. Kovler, The national survey of natural radioactivity in concrete produced in Israel, J. Environ. Radioact. 168 (2017) 46–53.

[16] M.P. Campos, L.J.P. Costa, M.B. Nisti, B.P. Mazzilli, Phosphogypsum recycling in the building materials industry: assessment of the radon exhalation rate, J. Environ. Radioact. 172 (2017) 232–236.

[17] M. Rafique, S.U. Rahman, T. Mahmood, S. Rahman, Matiullah S.U., Rehman Radon exhalation rate from soil, sand, bricks, and sedimentary samples collected from Azad Kashmir, Pakistan, Russ. Geol. Geophys. 52 (2011) 450–457.

[18] J. Porstenörfen, Properties and behaviour of Radon and Thoron and their decay products in the air, J. Aerosol Sc. 25, 2 (1994) 219–263.

[19] World Health Organization. WHO Report on the Global Tobacco Epidemic-The MPOWER package. WHO; Geneva (2008).

[20] M. Dondi, M. Marsigli, B. Fabbri, Recycling of industrial and urban wastes in brick production – A review, Tile Brick Int. 13 (1997) 218–225.

[21] M. Dondi, M. Marsigli, B. Fabbri, Recycling of industrial and urban wastes in brick production – A review (Part 2), Tile Brick Int. 13 (1997) 302–309.

[22] P. Duminuco, B. Messiga, M.P. Riccardi, Firing process of natural clays. Some microtextures and related phase compositions, Thermochim. Acta 321 (1998) 185–190.

[23] M.P. Riccardi, B. Messiga, P. Duminuco, An approach to the dynamics of clay firing, Appl. Clay Sci. 15 (1999) 393–409.

[24] G. Cultrone, E. Sebastián, Fly ash addition in clayey materials to improve the quality of solid bricks, Constr. Build. Mater. 23 (2009) 1178–1184.

[25] L. Zhang, Production of bricks from waste materials – A review, Constr. Build. Mater. 47 (2013) 643–655.

[26] P. Muñoz Velasco, M.P. Morales Ortíz, M.A. Mendívil Giró, L. Muñoz Velasco Fired clay bricks manufactured by adding wastes as sustainable construction material – A review, Constr. Build. Mater. 63 (2014) 97–107.

[27] C. Coletti, G. Cultrone, L. Maritan, C. Mazzoli, How to face the new industrial challenge of compatible, sustainable brick production: Study of various types of commercially available bricks, Appl. Clay Sci. 124–125 (2016) 219–226.

[28] S.M. Saleem Kazmi, M.J. Munir, Y.F. Wu, A. Hanif, I. Patnaikuni, Thermal performance evaluation of eco-friendly bricks incorporating waste glass sludge, J. Clean. Prod. 172 (2018) 1867–1880.

[29] E. Franzoni, Materials selection for green buildings: which tools for engineers and architects?, Procedia Eng. 21 (2011) 883–890.

[30] C. Coletti, L. Maritan, G. Cultrone, A. Hein, M.C. Dalconi, E. Molina C. Mazzoli, Recycling trachyte waste from quarry to brick industry: effects on petrophysical properties and durability of new bricks, Constr. Build. Mater.166 (2018) 792–807.

[31] R.M. Amin, A study of radon emitted from building materials using solid state nuclear track detectors, J. Radiat. Res. Appl. Sci. 8 (2015) 516–522.

[32] C. Coletti, G. Cultrone, L. Maritan, C. Mazzoli, Combined multi-analytical approach for study of pore system in bricks: How much porosity is there?, Mater. Charact. 121 (2016) 82–92.

[33] J. Labrincha, F. Pueras, W. Schroeyers, K. Kovler, Y. Pontikes, C. Nuccetelli, P. Krivenko, O. Kovalchuk, O. Petropavlovsky, M. Komljenovic, E. Fidanchevchki, R. Wiegers, E. Volceanov, E. Gunay, M.A. Sanjuán, V. Ducman, B. Angjusheva, D. Bajare, T. Kovacs, G. Bator, S. Schreurs, J. Aguiar, J.L. Provis, From NORM by-products to building materials, Naturally Occurring Radioactive Materials in Construction, Integrating Radiation Protection in Reuse, (COST Action Tu1301 Norm4building), Edit by Wouter Schroeyers, Woodhead Publishing (2017) 183–252.

[34] European Union (2013). Council Directive 2013/59/Euratom of 5 December 2013 laying down basic safety standards for protection against the dangers arising from exposure to ionising radiation, and repealing Directives 89/618/Euratom, 90/641/Euratom, 96/29/Euratom, 97/43/ Euratom and 2003/122/Euratom. Official Journal of the European Union, OJ L13, 17.01.2014, pp. 1–73.

[35] C. Coletti, L. Maritan, G. Cultrone, C. Mazzoli, Use of industrial ceramic sludge in brick production: Effect on aesthetic quality and physical properties, Constr. Build. Mater. 124 (2016) 219–227.

[36] M.F. Attallah, M.A. Hilal, S.I. Moussa, Quantification of some elements of nuclear and industrial interest from zircon mineral using neutron activation analysis and passive gamma-ray Spectroscopy, Appl. Radiat. Isotopes 128 (2017) 224–230.

[37] L. Tositti, G. Cinelli, E. Brattich, A. Galgaro, D. Mostacci, C. Mazzoli, M. Massironi, R. Sassi, Assessment of lithogenic radioactivity in the Euganean Hills magmatic district (NE Italy), J. Environ. Radioact. 166 (2017) 259–269..

[38] V.D. Scott, G. Love, Quantitative Electron Probe Microanalysis. John Wiley and Sons, New York (1983).

[39] G. Chen, J. Wang, The preparation of marine geological certified reference materials - polymetallic nodule GSPN-1 and marine sediment GSMS-1 from the Central Pacific Ocean, Geostand. Geoanal. Res. 22 (1998) 119–125.

[40] G. Cinelli, L. Tositti, B. Capaccioni, E. Brattich, D. Mostacci, Soil gas radon assessment and development of a radon risk map in Bolena, Central Italy, Environ. Geochem. Health 37 (2014) 305–319.

[41] G. Gilmore, “Practical gamma-ray Spectroscopy” 2nd edition, Wiley (2008).

[42] D.C. Stromswold, Calibration facilities for borehole and surface environmental radiation measurements, J. Radioanal. Nucl. Ch. 194 (1995) 393–401.

[43] Nordic, 2000. Naturally occurring Radiation in Nordic Countries—Recommendation. In: The Flag-Book series, The Radiation Protection Authorities in Denmark, Finland, Norway and Sweden, Reykjavik.

[44] S. Righi, L. Bruzzi, Natural radioactivity and radon exhalation in building materials used in Italian dwellings, J. Environ. Radioact. 88 (2006) 158–170.

[45] J. Beretka, P.J. Matthew, Natural radioactivity of Australian building materials, industrial wastes and by-products, Health Phys. 48 (1985) 87–95.

[46] L. Germinario, J.H. Hanchar, R. Sassi, L. Maritan, R. Cossio, A. Borghi, C. Mazzoli, New petrographic and geochemical tracers for recognizing the provenance quarry of trachyte of the Euganean Hills, northeastern Italy, Geoarchaeology 33 (2018) 430–452.

[47] G. Cultrone, E. Sebastián, K. Elert, M.J. de la Torre, O. Cazalla, C. Rodriguez-Navarro, Influence of mineralogy and firing temperature in the porosity of bricks, J. Eur. Ceram. Soc. 34 (2004) 547–564.

[48] L. Damonte, P. Rivas, A. Pasquevich, F. Andreola, F. Bondioli, A. M. Ferrari, L. Tositti, G. Cinelli, Structural Characterization of natural and processed zircons with X-rays and nuclear techniques, Adv. Condens. Matter Phys. (2017) 1–9.

[49] A. Sakoda, Y. Nishiyama, K. Hanamoto, Y. Ishimori, Y. Yamamoto, T. Kataoka, A. Kawabe, K. Yamaoka, Differences of natural radioactivity and radon emanation fraction among constituent minerals of rock or soil, Appl. Radiat. Isotopes 68 (2010) 1180–1184.

[50] G. Cultrone, C. Rodriguez-Navarro, E.M. Sebastián, O. Cazalla, M.J. de la Torre, Carbonate and silicate phase reactions during ceramic firing, Eur. J. Mineral. 13 (2001) 621–634.

[51] L. Maritan, L. Nodari, C. Mazzoli, A. Milano, U. Russo, Influence of firing conditions in ceramic products: experimental study on clay rich in organic matter, Appl. Clay Sci. 31 (2006) 1–15.

[52] R. Trevisi, S. Risica, M. D'Alessandro, D. Paradiso, C. Nuccetelli, Natural radioactivity in building materials in the European Union: a database and an estimate of radiological significance, J. Environ. Radioact. 105 (2012) 11–20.

[53] G. De With, P. de Jong, A. Röttger, Measurement of thoron exhalation rate from building materials, Health Phys. 7, Volume 107, Number 3 (2014) 206–212.

[54] R. Trevisi, F. Leonardi, S. Risica, C. Nuccetelli, Updated database on natural radioactivity in building materials in Europe, J. Environ. Radioact. 187 (2018) 90–105.

[55] Z. Sas, J. Somlai, G. Szeiler, T. Kovács, Radon emanation and exhalation characteristics of heat-treated clay samples, Radiat. Prot. Dosim. 152 (2012) 51–54.

[56] M. Marocchi, S. Righi, G.M. Bargossi, G. Gasparotto, Natural radionuclides content and radiological hazard of commercial ornamental stones: an integrated radiometric and mineralogical-petrographic study, Radiat. Meas. 46 (2011) 538–545.

[57] T. Kovacs, G. Bator, W. Schroeyers, J. Labrincha, F. Puertas, M. Hegedus, D. Nicolaides, M.A. Sanjuán, P. Krivenko, I.N. Grubeša, Z. Sas, B. Michalik, M. Anagnostakis, I. Barisic, C. Nuccetelli, R. Trevisi, T. Croymans, S. Schreurs, N. Todorović, D. Vaiciukyniene, R. Bistrickaite, A. Tkaczyk, K. Kovler, R. Wiegers, R. Doherty, From raw materials to NORM by-products, Naturally Occurring Radioactive Materials in Construction (2017) 135–182.

[58] Z. Sas, N. Vandevenne Rory Doherty, R. Vinai, J. Kwasny, M. Russell, W. Sha, M. Soutsos, W. Schroeyers, Radiological evaluation of industrial residues for construction purposes correlated with their chemical properties, Sci. Total Environ. 658 (2019) 141–151.

[59] W.W. Nazaroff, A.V. Nero Jr., Radon and Its Decay Products in Indoor Air. Wiley, New York (1988).

[60] L. Germinario, G.F. Andriani, R. Laviano, Decay of calcareous building stone under the combined action of thermoclastism and cryoclastism: A laboratory simulation, Constr. Build. Mater. 75 (2015) 385–394.

[61] C. Di Benedetto, P. Cappelletti, M. Favaro, S.F. Graziano, A. Langella, D. Calcaterra, A. Colella Porosity as key factor in the durability of two historical building stones: Neapolitan Yellow Tuff and Vicenza Stone, Eng Geol. 193 (2015) 310–319.

[62] S. Scrivano, L. Gaggero, J.G. Aguilar Micro-porosity and minero-petrographic features influences on decay: Experimental data from four dimension stones, Constr. Build. Mater. 173 (2018) 342–349.

[63] A.B. Tanner, Radon migration in the ground. In the Natural Radiation Environment, Houston, TX (1978).

[64] N.M. Hassan, M. Hosoda, T. Ishikawa, A. Sorimachi, S.K. Sahoo, S. Tokonami, M. Fukushi, Radon Migration Process and Its Influence Factors; Review. Jpn. J. Health Phys. 44 (2) (2009) 218–231.

[65] T.M. Semkow, P.P. Parekh, The role of radium distribution and porosity in radon emanation from soils, Geophys. Res. Lett. Vol. 17, no. 6, (1990) 837–840.

[66] S.A. Mujahid, S. Hussain, A.H. Dogar, S. Karim, Determination of porosity of different materials by radon diffusion, Radiat. Meas. 40 (2005) 106–109.

[67] H. Giesche, Mercury Porosimetry: A General (Practical) Overview. Part. Part. Syst. Charact. 23 (2006) 9–19.

[68] D.A.W. Bossus, Emanating power and specific surface area, Radiat. Prot. Dosimetry v. 7 (1984) 73–76.

[69] D.L. Whitney, B.W. Evans Abbreviations for names of rock-forming minerals, Am. Mineral. 95 (2010) 185–187.

**Table headings**

**Table 1:** Raw materials (clayey materials, temper and additives) and bricks production recipe (with relative firing temperature).

**Table 2:** Chemical composition of raw materials and bricks, expressed in wt. % of oxides for the major and minor elements and Loss On Ignition (LOI), and trace elements expressed in ppm. < DL: below the detection limit. *: not measured.

**Table 3:** Mineralogical composition of clayey materials, temper, additive and bricks determined by XRPD. Mineral abbreviations after Whitney and Evans (2010) [69]: Qz = quartz; Pl = plagioclase; Afs = alkali-feldspar; Cal = calcite; Dol = dolomite; Ilt = illite; Chl = chlorite; Bt = Biotite; Hem = hematite; Hsm = hausmannite; Crs = Cristobalite; Mul = mullite; Di = diopside; Gh = gehlenite;

Wo = wollastonite; Bst = bustamite; Kln = kaolinite; Crd = cordierite; AM = amorphous. Estimated relative abundance: **** = very abundant; *** = abundant; ** = medium; * = scarce; + = rare; - = absent.

**Table 4:** Natural radioactivity in raw materials and bricks including activity concentrations of $^{226}Ra$, $^{232}Th$, and $^{40}K$ (Bq/kg) , concentration of elemental U, Th, and K (ppm) and Iα and I indexes and Ra_eq (Bq/kg). Experimental data below the Minimum Detectable Activity (MDA) are reported as <MDA as determined from spectrum processing.

**Table 5:** E-PERM results: $Q_A$, exhalation rate (Bq/d); *Ea*, surface exhalation rate (Bq/d·m$^2$); *Em*, mass exhalation rate (Bq/d·kg); η, emanation coefficient.

**Table 6:** Physical parameters. MIP results: $\varepsilon_{tot}$, total open porosity (%); $\rho_r$, bulk/real density (kg/m); $\rho_a$, apparent density (kg/m); $\varepsilon_{<0.1\mu m}$, open porosity < 0.1μm (%); $\varepsilon_{<1\mu m}$, open porosity < 1μm (%); $\varepsilon_{>1\mu m}$, open porosity > 1μm (%); $\varepsilon_{0.1\text{-}1\mu m}$, open porosity between 0.1 and 1 μm (%). $N_2$ adsorption: $S_{aBET}$, BET surface area (m$^2$/g). MIP: $S_{aMIP}$, MIP surface area (m$^2$/g); $S_{aMIP<0.05\mu m}$, surface area for pores < 0.05 μm (m$^2$/g); $S_{aMIP<0.5\mu m}$, surface area for pores < 0.5 μm (m$^2$/g).

**List of Figures**

**Figure 1:** a) Dendrogram of cluster analysis according to average linkage method and square Euclidean distance; b) score and loading plot of the principal component analysis performed on the XRF chemical data of the studied bricks. PC1, PC2 and PC3 cover 41.3%, 30.8% and 12.2% (total 84.3%) of the total variance, respectively.

**Figure 2:** Correlation between radon mass exhalation rate (*Em*) versus: a) mass emission ($Em_{\varepsilon}$) normalised for total porosity considering all the studied bricks; b) mass emission ($Em_{CRa}$) normalised for $^{226}Ra$ concentration considering all the studied bricks.

**Figure 3:** a) correlation between measured radon mass exhalation rate *Em* (Bq/d·kg) and total porosity ε (%); b) correlation between measured radon mass exhalation rate *Em* (Bq/d·kg) and open porosity < 0.1μm $\varepsilon_{<0.1\mu m}$ (%); c) correlation between measured radon mass exhalation rate *Em* (Bq/d·kg) and surface area $S_{aMIP}$, determined by MIP measurements, ($m^2/g$); d) correlation between measured radon mass exhalation rate *Em* (Bq/d·kg) and surface area $S_{aBET}$, determined by BET measurements ($m^2/g$); e) correlation between measured radon mass exhalation rate *Em* (Bq/d·kg) and surface area for pores < 0.05 μm $S_{aMIP<0.05\mu m}$, determined by MIP measurements, ($m^2/g$); f) correlation between measured radon mass exhalation rate *Em* (Bq/d·kg) and surface area for pores < 0.5 μm $S_{aMIP<0.5\mu m}$, determined by MIP measurements ($m^2/g$).

**Figure 4:** Scores and loading plots of PCA performed on the following variables: Iα index; I index; the major elements $SiO_2$, $TiO_2$, $Al_2O_3$, $Fe_2O_3$, CaO, MgO, MnO, $Na_2O$, $K_2O$ and $P_2O_5$ (expressed as wt. %); the trace elements Zr, Rb, Sr, Pb, Cr, Ni and Zn (expressed as ppm); LOI (Lost On Ignition, wt. %); $\varepsilon_{tot}$, total open porosity (%); $\rho_r$, real density ($kg/m^3$); $\varepsilon_{<0.1\mu m}$, open porosity < 0.1μm (%); $S_{aBET}$, BET surface area ($m^2/g$); $S_{aMIP}$, MIP surface area ($m^2/g$); *Em*, radon mass exhalation rate (Bq/d·kg); *Ea*, radon surface exhalation rate (Bq/ d·$m^2$); $C_{Ra}$, activities of $^{226}Ra$ (Bq/kg) PC1, PC2 and PC3 representing 34.7%, 26.9% and 16.4% of total variance, respectively.

**Supplementary material:**

**Figure 1S:** XRPD pattern of sample PIR. Mineral abbreviations as in Table 3.

Table 1



| | sample | type | |
|---|---|---|---|
| raw materials | LG | Clay | |
| | LRS | Clay | |
| | LRSS | Clay | |
| | LRSSF | Clay | |
| | SS | Standard temper (quartz-rich sand) | |
| | TR | Temper (waste 1 = trachyte by-product from quarry) | |
| | F | Temper (waste 2 = sludge from ceramic industry) | |
| | PIR | Temper (waste 3 = sludge from ceramic industry) | |
| | MN | Dye additive ($Mn_2O_3$, hausmannite) | |
| | brick | mix design | firing T (°C) |
| commercial bricks | GP | Clay LG + siliceous temper (10 wt. %) | 1050 |
| | N | Clay LG + siliceous temper (10 wt. %) + MN (15 wt. %) | 1050 |
| | RSS | Clay LRSS + siliceous temper (10 wt. %) | 950 |
| | R6 | Clay LRSS + siliceous temper (10 wt. %) | 600 |
| | RS | Clay LRS + siliceous temper (10 wt. %) | 980 |
| | RCF | Clay LRSSF + siliceous temper (10 wt. %) | 1050 |
| bricks made with trachyte waste | B5.9 | Clay LRSSF + temper TR (5 wt. %) | 900 |
| | B5.10 | Clay LRSSF + temper TR (5 wt. %) | 1000 |
| | B5.11 | Clay LRSSF + temper TR (5 wt. %) | 1100 |
| | B10.9 | Clay LRSSF + temper TR (10 wt. %) | 900 |
| | B10.10 | Clay LRSSF + temper TR (10 wt. %) | 1000 |
| | B10.11 | Clay LRSSF + temper TR (10 wt. %) | 1100 |
| | B15.9 | Clay LRSSF + temper TR (15 wt. %) | 900 |
| | B15.10 | Clay LRSSF + temper TR (15 wt. %) | 1000 |
| | B15.11 | Clay LRSSF + temper TR (15 wt. %) | 1100 |
| bricks made with ceramic sludge | FM | Clay LG + temper F (10 wt. %) | 1050 |
| | B_PIR | Clay LG + temper PIR (10 wt. %) | 1050 |

Table 2



| | | $SiO_2$ | $Al_2O_3$ | $Fe_2O_3$ | MnO | MgO | CaO | $Na_2O$ | $K_2O$ | $TiO_2$ | $P_2O_5$ | LOI | Zr | Rb | Sr | Pb | Cr | Ni | Zn |
|---|---|---|---|---|---|---|---|---|---|---|---|---|---|---|---|---|---|---|---|
| raw materials | LG | 39.81 | 10.63 | 3.87 | 0.08 | 4.75 | 17.76 | 0.54 | 2.37 | 0.43 | 0.11 | 19.65 | 116 | 81 | 157 | 17 | 74 | 46 | 69 |
| | LRS | 51.50 | 12.72 | 4.43 | 0.09 | 3.41 | 10.45 | 0.70 | 2.74 | 0.54 | 0.12 | 13.29 | 147 | 98 | 116 | 22 | 89 | 42 | 77 |
| | LRSS | 57.77 | 14.14 | 4.85 | 0.10 | 2.68 | 6.16 | 1.09 | 2.99 | 0.63 | 0.13 | 9.47 | 167 | 106 | 86 | 27 | 89 | 36 | 85 |
| | LRSSF | 63.57 | 13.62 | 5.06 | 0.11 | 2.29 | 3.85 | 0.96 | 2.61 | 0.84 | 0.13 | 6.94 | 186 | 96 | 87 | 24 | 115 | 45 | 80 |
| | TR | 65.27 | 16.59 | 3.26 | 0.07 | 0.61 | 1.74 | 5.06 | 5.06 | 0.65 | 0.18 | 0.92 | 674 | 114 | 239 | 18 | <DL | 1 | 83 |
| | F | 72.52 | 18.36 | 1.20 | 0.01 | 0.51 | 1.00 | 3.11 | 2.31 | 0.71 | 0.11 | 0.16 | 1583 | * | * | * | * | * | * |
| | PIR | 65.68 | 17.83 | 2.07 | 0.03 | 0.65 | 2.19 | 3.37 | 1.85 | 0.60 | 0.16 | 4.35 | 7157 | 211 | 567 | 77 | 2201 | 37 | 4915 |
| commercial bricks | GP | 50.17 | 13.19 | 4.80 | 0.09 | 5.61 | 20.39 | 0.72 | 2.84 | 0.49 | 0.13 | 1.56 | 128 | 100 | 187 | 20 | 83 | 58 | 80 |
| | N | 42.42 | 11.67 | 4.93 | 12.86 | 4.93 | 17.63 | 0.60 | 2.66 | 0.52 | 0.15 | 1.63 | 127 | 90 | 162 | 48 | 76 | 56 | 193 |
| | RSS | 63.79 | 15.28 | 5.16 | 0.11 | 2.87 | 7.01 | 0.99 | 3.20 | 0.66 | 0.13 | 0.78 | 164 | 118 | 105 | 28 | 90 | 41 | 91 |
| | R6 | 60.32 | 14.35 | 4.85 | 0.11 | 2.69 | 6.22 | 0.93 | 3.03 | 0.64 | 0.13 | 6.74 | 149 | 105 | 94 | 25 | 93 | 40 | 81 |
| | RS | 59.46 | 14.53 | 4.94 | 0.09 | 3.69 | 11.06 | 0.89 | 2.99 | 0.59 | 0.13 | 1.62 | 143 | 109 | 135 | 25 | 93 | 51 | 87 |
| | RCF | 65.29 | 13.81 | 5.41 | 0.10 | 3.06 | 6.52 | 1.52 | 2.41 | 0.72 | 0.15 | 1.01 | 201 | 124 | 181 | 38 | 18 | 78 | 117 |
| bricks made with trachyte waste | B5.9 | 64.06 | 13.92 | 5.44 | 0.12 | 3.06 | 6.74 | 1.86 | 2.39 | 0.68 | 0.17 | 1.56 | 258 | 121 | 218 | 36 | 174 | 108 | 108 |
| | B5.10 | 64.23 | 14.12 | 5.50 | 0.12 | 3.16 | 6.73 | 1.88 | 2.41 | 0.69 | 0.18 | 0.99 | 234 | 121 | 222 | 34 | 256 | 131 | 102 |
| | B5.11 | 64.99 | 14.05 | 5.48 | 0.12 | 3.13 | 6.76 | 1.92 | 2.42 | 0.68 | 0.17 | 0.28 | 233 | 122 | 215 | 38 | 160 | 110 | 104 |
| | B10.9 | 63.89 | 14.24 | 5.45 | 0.11 | 2.98 | 6.21 | 2.07 | 2.58 | 0.69 | 0.18 | 1.60 | 265 | 124 | 224 | 32 | 162 | 108 | 289 |
| | B10.10 | 64.34 | 14.35 | 5.43 | 0.10 | 2.97 | 6.27 | 2.09 | 2.58 | 0.69 | 0.18 | 0.99 | 259 | 125 | 219 | 35 | 165 | 103 | 104 |
| | B10.11 | 64.82 | 14.47 | 5.52 | 0.12 | 3.03 | 6.29 | 2.09 | 2.62 | 0.71 | 0.18 | 0.15 | 257 | 126 | 223 | 38 | 170 | 110 | 102 |
| | B15.9 | 64.55 | 14.40 | 5.35 | 0.12 | 2.81 | 5.96 | 2.27 | 2.71 | 0.70 | 0.18 | 0.93 | 282 | 125 | 227 | 34 | 155 | 93 | 104 |
| | B15.10 | 64.41 | 14.58 | 5.35 | 0.11 | 2.84 | 5.99 | 2.31 | 2.75 | 0.72 | 0.18 | 0.75 | 285 | 125 | 230 | 30 | 157 | 95 | 105 |
| | B15.11 | 65.04 | 14.55 | 5.42 | 0.11 | 2.89 | 5.94 | 2.30 | 2.72 | 0.72 | 0.19 | 0.13 | 272 | 125 | 223 | 37 | 143 | 95 | 105 |
| bricks made with ceramic sludge | FM | 53.88 | 13.40 | 4.18 | 0.08 | 5.06 | 17.85 | 1.43 | 2.58 | 0.53 | 0.12 | 0.89 | 323 | 122 | 235 | 33 | 111 | 56 | 360 |
| | B_PIR | 54.64 | 14.11 | 3.79 | 0.26 | 4.53 | 16.67 | 1.79 | 2.40 | 0.53 | 0.13 | 1.14 | 2032 | 132 | 335 | 131 | 462 | 41 | 1192 |

Table 3

Click here to access/download;Table;Table 3.docx

| | | Qz | Ilt | Chl | Afs | Pl | Cal | Dol | Hem | Crs | Hsm | Mul | Kln | Bt | AM |
|---|---|---|---|---|---|---|---|---|---|---|---|---|---|---|---|
| raw materials | LG | **** | ** | ** | * | * | **** | *** | + | | - | - | - | - | - |
| | LRS | **** | ** | ** | * | ** | ** | ** | + | | - | - | - | - | - |
| | LRSS | **** | ** | ** | ** | ** | * | * | + | | - | - | - | - | - |
| | LRSSF | **** | ** | ** | ** | ** | + | + | + | | - | - | - | - | - |
| | TR | ** | - | - | *** | *** | - | - | - | | - | - | - | * | |
| | F | **** | - | - | - | *** | - | - | - | + | - | ** | - | - | ** |
| | PIR | **** | * | - | ** | *** | * | - | - | | - | - | * | - | - |
| | MN | - | - | - | - | - | - | - | - | | **** | - | - | - | - |

| | | Qz | Ilt | Chl | Afs | Pl | Cal | Dol | Hem | Wo | Di | Gh | Bst | Crd | Bt | AM |
|---|---|---|---|---|---|---|---|---|---|---|---|---|---|---|---|---|
| commercial bricks | GP | **** | - | - | ** | * | - | - | * | ** | *** | *** | - | - | - | ** |
| | N | **** | - | - | ** | * | - | - | * | ** | *** | *** | *** | - | - | *** |
| | RSS | **** | - | - | * | ** | - | - | * | * | + | + | - | - | - | - |
| | R6 | **** | ** | ** | * | *** | ** | ** | * | - | - | - | - | - | - | - |
| | RS | **** | - | - | * | ** | - | - | * | * | * | * | - | - | - | - |
| | RCF | **** | - | - | * | ** | - | - | * | * | * | ** | - | - | - | - |
| bricks made with trachyte waste | B5.09 | **** | * | - | ** | ** | + | - | * | - | * | * | - | + | + | ** |
| | B5.10 | **** | + | - | ** | ** | + | - | * | - | * | ** | - | - | + | ** |
| | B5.11 | **** | - | - | ** | ** | - | - | * | - | * | *** | - | - | + | *** |
| | B10.09 | **** | + | - | ** | ** | + | - | * | - | * | * | - | + | + | * |
| | B10.10 | **** | + | - | ** | ** | + | - | * | - | * | ** | - | - | + | * |
| | B10.11 | **** | - | - | ** | ** | - | - | * | - | * | *** | - | - | + | *** |
| | B15.09 | **** | * | - | *** | *** | + | - | * | - | * | * | - | + | ++ | * |
| | B15.10 | **** | + | - | *** | *** | + | - | * | - | * | ** | - | - | ++ | * |
| | B15.11 | **** | - | - | *** | *** | - | - | * | - | * | *** | - | - | ++ | ** |
| bricks made with ceramic sludge | FM | **** | - | - | ** | ** | - | - | - | * | ** | ** | - | - | - | **** |
| | B_PIR | **** | - | - | * | *** | - | - | + | * | *** | *** | - | - | - | ** |

Table 4



| | | $^{226}$Ra (Bq/kg) | σ% | $^{232}$Th (Bq/kg) | σ% | $^{40}$K (Bq/kg) | σ% | U (ppm) | σ | Th (ppm) | σ | K (wt.%) | σ | I | Iα | Ra_eq (Bq/kg) |
|---|---|---|---|---|---|---|---|---|---|---|---|---|---|---|---|---|
| raw materials | LG | 31 | 11 | 37 | 7 | 526 | 3 | 3 | - | 9 | - | 2 | - | 0.47 | 0.16 | 125 |
| | LRS | 29 | 17 | 34 | 10 | 633 | 6 | 2 | - | 8 | - | 2 | - | 0.48 | 0.14 | 126 |
| | LRSS | 50 | 12 | 59 | 10 | 716 | 6 | 4 | - | 14 | 1 | 2 | - | 0.70 | 0.25 | 189 |
| | LRSSF | 34 | 21 | 44 | 7 | 491 | 4 | 3 | 1 | 11 | - | 2 | - | 0.50 | 0.17 | 135 |
| | SS | - | - | - | 13 | 279 | 6 | - | - | 1 | - | 1 | - | - | - | 30 |
| | TR | 52 | 6 | 50 | 3 | 1210 | 2 | 4 | - | 12 | - | 4 | - | 0.82 | 0.26 | 216 |
| | F | - | - | <8 | - | <58 | - | - | - | - | - | - | - | - | - | - |
| | PIR | 120 | 6 | 41 | 6 | 511 | 6 | 10 | 1 | 10 | 1 | 2 | - | 0.78 | 0.60 | 219 |
| | MN | - | - | <7 | - | <47 | - | - | - | - | - | - | - | - | - | - |
| commercial bricks | GP | 45 | 14 | 47 | 9 | 700 | 3 | 4 | 1 | 11 | 1 | 2 | - | 0.62 | 0.22 | 161 |
| | N | 29 | 17 | 43 | 7 | 654 | 6 | 2 | - | 11 | 1 | 2 | - | 0.53 | 0.15 | 137 |
| | RSS | 41 | 14 | 52 | 7 | 757 | 3 | 3 | - | 13 | 1 | 2 | - | 0.65 | 0.21 | 168 |
| | R6 | 41 | 13 | 50 | 6 | 719 | 3 | 3 | - | 12 | 1 | 2 | - | 0.62 | 0.20 | 162 |
| | RS | 36 | 17 | 44 | 6 | 755 | 2 | 3 | 1 | 11 | 1 | 2 | - | 0.60 | 0.18 | 151 |
| | RCF | 43 | 13 | 46 | 7 | 666 | 3 | 3 | - | 11 | 1 | 2 | - | 0.60 | 0.21 | 156 |
| bricks made with trachyte waste | B5.9 | 55 | 12 | 56 | 8 | 1016 | 6 | 4 | 1 | 14 | 1 | 3 | - | 0.80 | 0.27 | 206 |
| | B5.10 | 50 | 11 | 43 | 7 | 614 | 3 | 4 | - | 11 | 1 | 2 | - | 0.59 | 0.23 | 155 |
| | B5.11 | 47 | 17 | 66 | 8 | 1000 | 6 | 3 | 1 | 16 | 1 | 3 | - | 0.82 | 0.24 | 212 |
| | B10.9 | 46 | 7 | 45 | 4 | 663 | 2 | 4 | - | 11 | 1 | 2 | - | 0.60 | 0.23 | 157 |
| | B10.10 | 51 | 12 | 44 | 8 | 693 | 3 | 4 | - | 11 | 1 | 2 | - | 0.62 | 0.25 | 163 |
| | B10.11 | 47 | 16 | 44 | 9 | 843 | 6 | 4 | 1 | 11 | 1 | 3 | - | 0.66 | 0.23 | 169 |
| | B15.9 | 46 | 10 | 43 | 6 | 689 | 3 | 4 | - | 11 | 1 | 2 | - | 0.59 | 0.23 | 155 |
| | B15.10 | 46 | 1 | 53 | 9 | 761 | 6 | 4 | - | 13 | 1 | 2 | - | 0.67 | 0.23 | 175 |
| | B15.11 | 47 | 17 | 66 | 8 | 1000 | 6 | 4 | - | 10 | 1 | 2 | - | 0.61 | 0.26 | 160 |
| bricks made with ceramic sludge | FM | 40 | 12 | 54 | 8 | 696 | 3 | 3 | 0.40 | 13 | 1 | 2 | - | 0.64 | 0.20 | 167 |
| | B_PIR | 55 | 9 | 46 | 12 | 599 | 6 | 4 | 0.41 | 11 | 1 | 2 | - | 0.61 | 0.28 | 163 |

Table 5



| | | Exhalation rate $Q_A$ (Bq/d) | Surface exhalation rate Ea (Bq/d·m$^2$) | Mass exhalation rate Em (Bq/d·kg) | Emanation coefficient η |
|---|---|---|---|---|---|
| commercial bricks | GP | 0.014 | 1.28 | 0.133 | 0.016 |
| | N | 0.019 | 1.87 | 0.179 | 0.034 |
| | RSS | 0.017 | 2.84 | 0.176 | 0.023 |
| | R6 | 0.084 | 8.58 | 0.803 | 0.109 |
| | RS | 0.016 | 1.65 | 0.153 | 0.024 |
| | RCF | 0.000 | 0.00 | 0.000 | 0.000 |
| bricks made with trachyte waste | B5.9 | 0.040 | 3.64 | 0.321 | 0.032 |
| | B5.10 | 0.015 | 0.96 | 0.143 | 0.016 |
| | B5.11 | 0.003 | 0.26 | 0.024 | 0.003 |
| | B10.9 | 0.029 | 2.96 | 0.275 | 0.033 |
| | B10.10 | 0.034 | 3.35 | 0.310 | 0.034 |
| | B10.11 | 0.024 | 2.80 | 0.266 | 0.031 |
| | B15.9 | 0.030 | 2.89 | 0.250 | 0.030 |
| | B15.10 | 0.013 | 1.52 | 0.113 | 0.014 |
| | B15.11 | 0.023 | 2.31 | 0.206 | 0.022 |
| bricks made with ceramic sludge | FM | 0.028 | 2.84 | 0.282 | 0.039 |
| | B_PIR | 0.022 | 2.23 | 0.222 | 0.022 |

Table 6



| | | $\varepsilon_{tot}$ (%) | $\rho_a$ (kg/m$^3$) | $\rho_r$ (kg/m$^3$) | $\varepsilon_{<0.1\,\mu m}$ (%) | $\varepsilon_{<1\mu m}$ (%) | $\varepsilon_{>1\mu m}$ (%) | $\varepsilon_{0.1\text{-}1\mu m}$ (%) | $S_{aBET}$ | $S_{aMIP}$ | $S_{aMIP<0.05\mu m}$ | $S_{aMIP<0.5\mu m}$ |
|---|---|---|---|---|---|---|---|---|---|---|---|---|
| commercial bricks | GP | 47.45 | 1400 | 2680 | 0.62 | 46.31 | 1.14 | 45.69 | 2.54 | 2.04 | 0.03 | 0.11 |
| | N | 46.87 | 1500 | 2870 | 0.83 | 46.02 | 0.86 | 45.18 | 4.33 | 2.57 | 0.04 | 0.10 |
| | RSS | 38.83 | 1540 | 2550 | 2.24 | 33.45 | 5.39 | 31.21 | 3.58 | 1.73 | 0.06 | 0.04 |
| | R6 | 34.20 | 1700 | 2580 | 8.55 | 31.06 | 3.21 | 22.51 | 10.24 | 7.05 | 0.14 | 0.03 |
| | RS | 42.25 | 1540 | 2660 | 2.86 | 39.90 | 2.35 | 37.04 | 5.32 | 2.37 | 0.08 | 0.06 |
| | RCF | 35.85 | 1700 | 2580 | 1.13 | 24.05 | 11.80 | 22.92 | 1.56 | 1.20 | 0.02 | 0.26 |
| Bricks made with trachyte waste | B5.9 | 25.22 | 1560 | 2090 | 3.16 | 20.37 | 4.86 | 17.21 | 2.11 | 2.94 | 0.12 | 0.02 |
| | B5.10 | 38.10 | 1590 | 2570 | 1.30 | 22.24 | 15.93 | 20.94 | 2.21 | 1.63 | 0.06 | 0.02 |
| | B5.11 | 34.40 | 1650 | 2520 | 0.93 | 16.80 | 17.67 | 15.87 | 0.63 | 0.90 | 0.05 | 0.02 |
| | B10.9 | 27.50 | 1570 | 2170 | 5.11 | 20.53 | 7.03 | 15.42 | 1.93 | 3.26 | 0.12 | 0.01 |
| | B10.10 | 38.39 | 1580 | 2560 | 1.73 | 23.39 | 15.00 | 21.66 | 0.98 | 1.57 | 0.07 | 0.02 |
| | B10.11 | 19.40 | 1610 | 2000 | 0.00 | 11.36 | 8.04 | 11.36 | 0.58 | 0.27 | 0.01 | 0.01 |
| | B15.9 | 23.22 | 1640 | 2140 | 4.10 | 19.17 | 4.05 | 15.07 | 1.48 | 3.44 | 0.13 | 0.01 |
| | B15.10 | 36.97 | 1600 | 2550 | 2.57 | 23.07 | 13.89 | 20.50 | 0.95 | 2.44 | 0.08 | 0.02 |
| | B15.11 | 27.58 | 1670 | 2310 | 0.53 | 14.68 | 12.90 | 14.15 | 0.50 | 0.60 | 0.03 | 0.01 |
| bricks made with ceramic sludge | FM | 49.57 | 1600 | 3100 | 2.61 | 47.21 | 2.36 | 44.60 | 1.99 | 1.07 | 0.08 | 0.32 |
| | B_PIR | 41.98 | 1460 | 2520 | 0.54 | 24.02 | 17.96 | 23.48 | 2.31 | 1.81 | 0.04 | 0.24 |

Figure 1

Click here to access/download;Figure;Fig. 1.eps

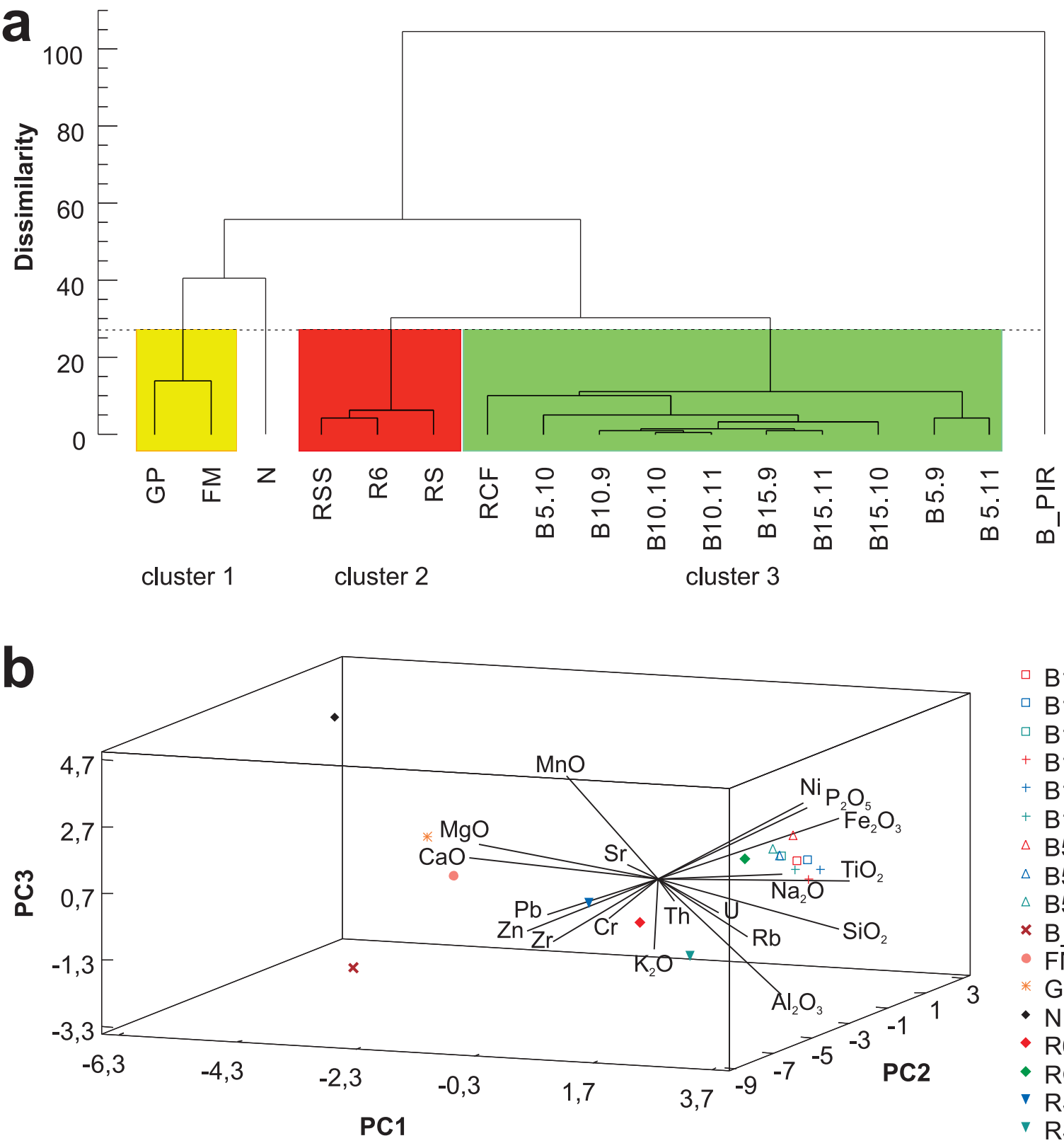

Figure 2

Click here to access/download;Figure;Fig. 2.eps

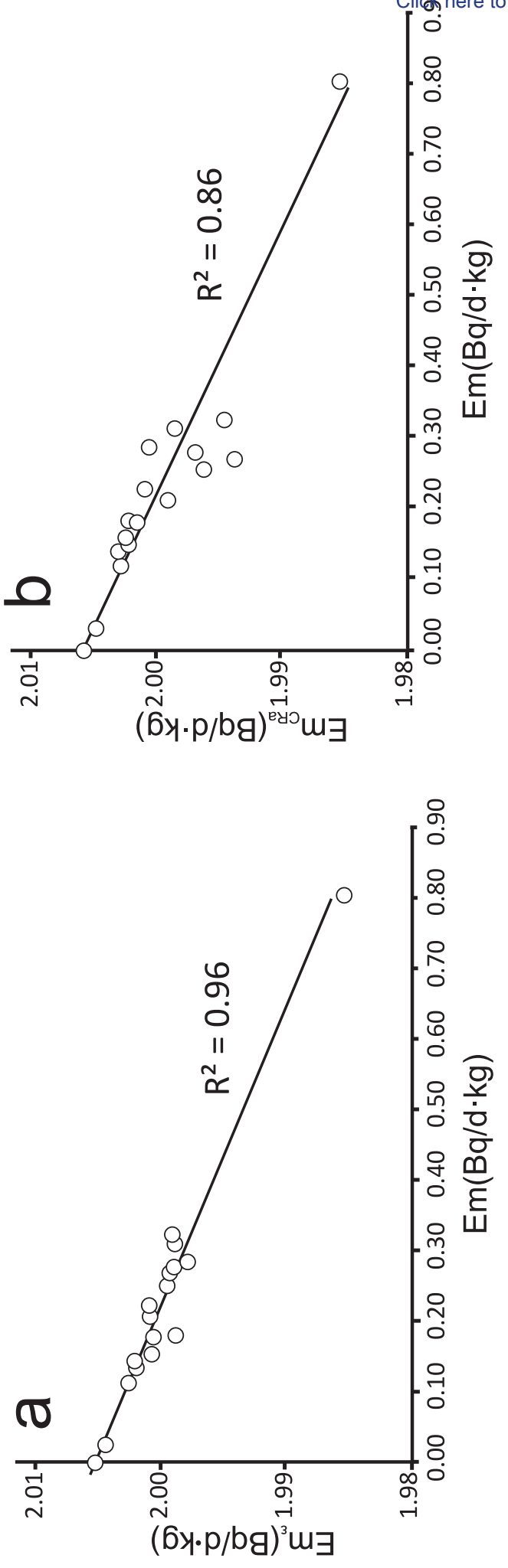

Figure 3

Click here to access/download;Figure;Fig. 3.eps

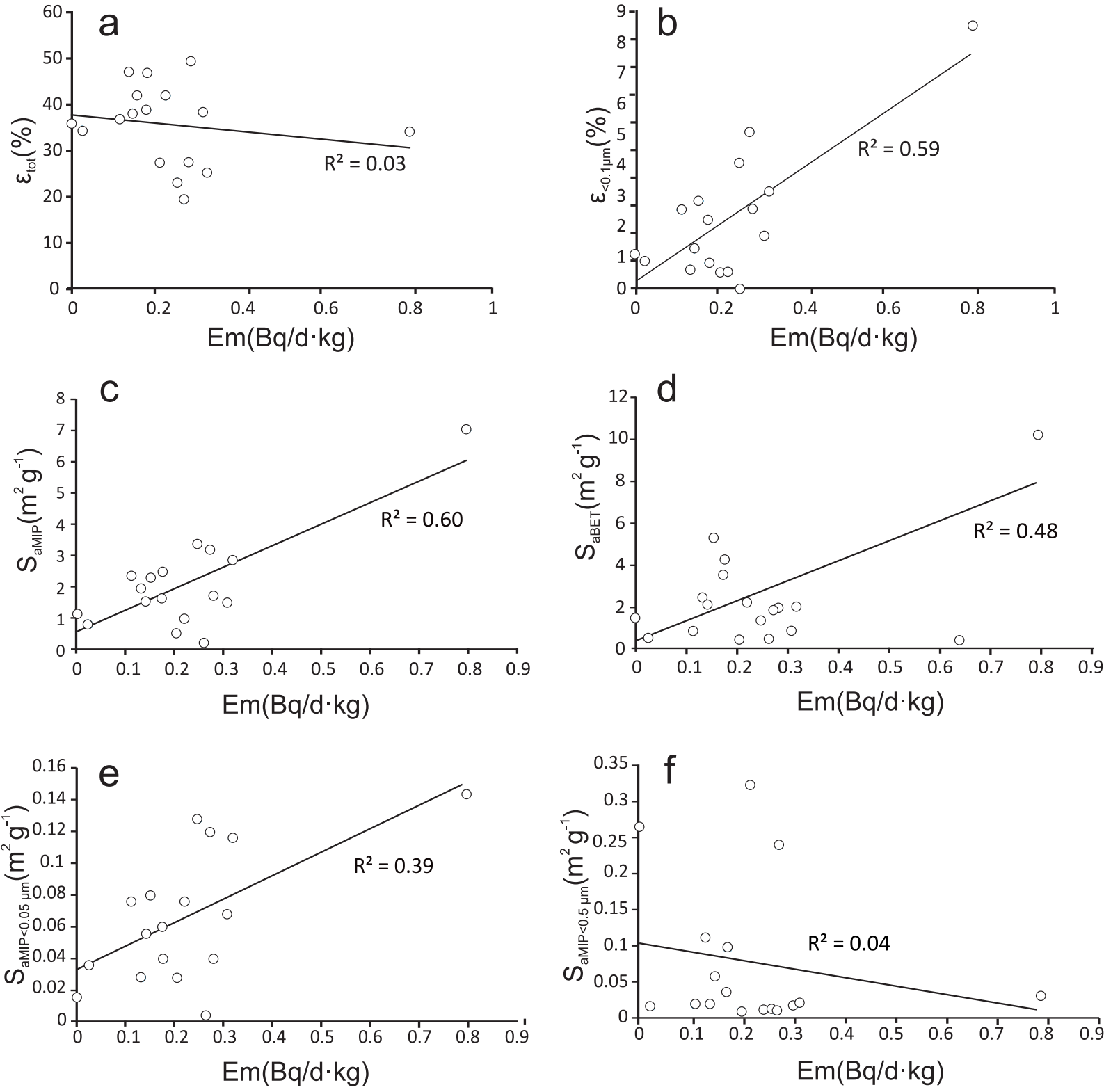

Figure 4

Click here to access/download;Figure;Fig. 4.eps

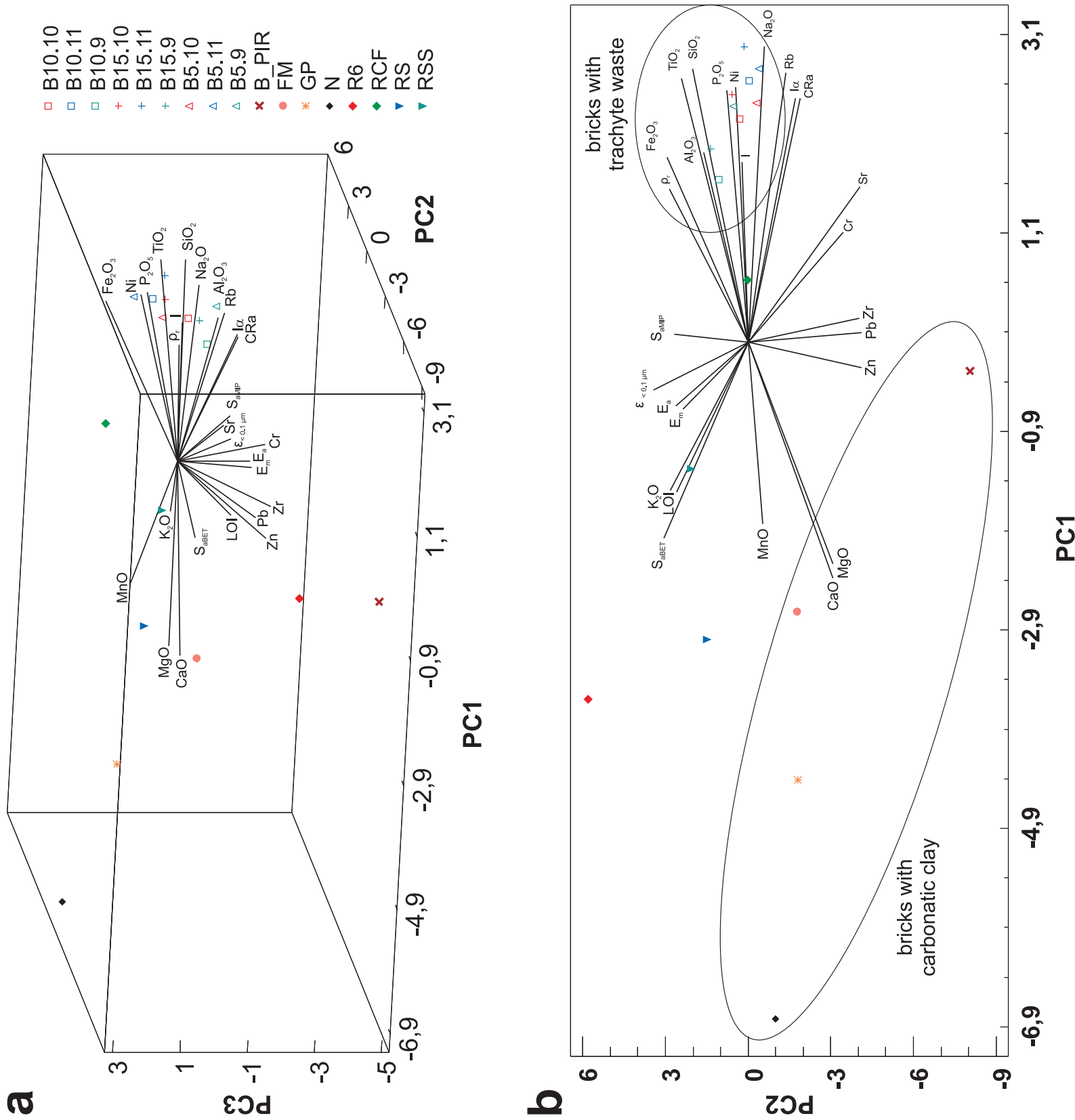

Figure 1S

Click here to access/download;Figure;Fig.1S.tif